

THE FORMATION OF H₂ IN VARIABLE HERBIG-HARO JETS

A. C. Raga,¹ D. A. Williams,² A. J. Lim³

Received 2004 November 15; accepted 2005 January 31

RESUMEN

Las cadenas de nudos alineados que definen los haces de los chorros HH a veces son observadas tanto en líneas atómicas/iónicas como en líneas moleculares (de H₂). Modelamos estos objetos como chorros con una velocidad de expulsión dependiente del tiempo, la cual produce superficies de trabajo internas que viajan a lo largo del chorro. Si esta interpretación es correcta, entonces la presencia de nudos alineados de H₂ es un indicador de alta sensibilidad de las amplitudes de la variabilidad en la expulsión. Encontramos que para variabilidades con amplitudes de $\sim 10 \text{ km s}^{-1}$, las superficies de trabajo internas tienen condiciones apropiadas para que se forme H₂ (mediante química de iones negativos y positivos en la fase gaseosa). Presentamos simulaciones axisimétricas hidrodinámicas+químicas que muestran que fracciones de H₂ de hasta $\sim 1\text{--}10\%$ pueden ser obtenidas, y que la emisión de H₂ 1–0 S(1) resultante puede ser substancialmente más alta que la emisión de H α . De nuestro estudio, concluimos que la emisión de H₂ observada en las cadenas de nudos de algunos chorros HH podrían corresponder a moléculas formadas *in situ* dentro de superficies de trabajo internas que viajan a lo largo del chorro.

ABSTRACT

The chains of aligned knots that define the beams of HH jets are sometimes observed both in atomic/ionic as well as in molecular (H₂) emission lines. We model such objects as jets with an ejection velocity time-variability, which produces internal working surfaces that travel down the jet beam. If this interpretation is indeed correct, then the presence of aligned H₂ knots is a sensitive indicator of the amplitude of the ejection velocity variability. We find that for variabilities with an amplitude of $\sim 10 \text{ km s}^{-1}$, the internal working surfaces have appropriate conditions for H₂ to be formed (via negative and positive ion gas phase chemistry). We present axisymmetric gasdynamic+chemical numerical simulations which show that H₂ fractions as high as $\sim 1\text{--}10\%$ can be obtained, and that the resulting H₂ 1–0 S(1) emission can be substantially larger than the H α emission. From our study, we conclude that the H₂ emission observed in the chains of knots along some HH jets could correspond to molecules formed *in situ* within the internal working surfaces that travel down the jet flow.

Key Words: **ISM: HERBIG-HARO OBJECTS — ISM: JETS AND OUTFLOWS — ISM: KINEMATICS AND DYNAMICS**

1. INTRODUCTION

Many Herbig-Haro (HH) flows have been detected in the IR rovibrational lines of H₂. Some of these objects show H₂ emission which appears to

be associated with the bow shock wings of the major working surfaces, in which the HH flow might be pushing shocks into the surrounding, molecular environment. This is the situation found in HH 1 (Davis, Smith, & Eislöffel 2000a), HH 47 (Fernandes 2000) and possibly also in HH 32 (Davis, Eislöffel & Smith 1996), though the interpretation of the emission from this object is complicated by the nearness of the outflow axis to the line of sight.

¹Instituto de Ciencias Nucleares, Universidad Nacional Autónoma de México, México, D. F., México.

²Department of Physics and Astronomy, University College London, UK.

³Department of Applied Mathematics, University of Leeds, UK.

Other HH flows, however, show H_2 emission that more closely follows the chains of aligned knots seen in optical and IR atomic/ionic lines, which appear to define the beam of the HH jet. An object which falls into this category is HH 110 (Reipurth & Olberg 1991, Reipurth, Raga, & Heathcote 1996), which shows an extended chain of H_2 features which lie directly to one side of the atomic/ionic jet (Davis, Mundt, & Eisloffel 1994; Noriega-Crespo et al. 1996). This H_2 emission has been interpreted as corresponding to molecular material which has been dragged by the HH jet as it interacts with the surface of a dense, molecular cloud core (Noriega-Crespo et al. 1996; Raga et al. 2002a).

Even though the offset between the atomic/ionic and molecular emission of HH 110 allows an interpretation of the H_2 as entrained molecular gas, other objects do not show such spatial offsets. For example, Gredel & Reipurth (1994) observed spatially coincident H_2 1–0 S(1) and [S II] 6716/30 emission in the chain of knots extending up to $\sim 30''$ away from the source along the HH 111 flow.

The best studied example of this kind of spatial coincidence appears to be the HH 1 jet. Reipurth et al. (2000) have compared *HST* WFPC and NICMOS images of this jet, and detect no difference either in the positions or the widths of the knots along the jet as seen in the H_2 2.12 μm and [Fe II] 1.64 μm emission lines. Likewise, in the region in which the knots are also detected in the [S II] and $H\alpha$ lines, no difference is seen between the H_2 and the atomic/ionic emission.

These observations represent an important challenge for models in which the molecular gas is interpreted as material entrained by an atomic/ionic jet flow (see Downes & Cabrit 2003 and references therein), as these models in practice predict that the molecular gas should be mostly confined to an envelope around the jet beam. As the observations of the HH 1 jet of Reipurth et al. (2000) resolve the cross section of the jet beam, they appear to eliminate the possibility of the existence of an “ H_2 envelope” surrounding the jet beam.

Another possibility for obtaining more effective entrainment of molecular gas into an HH flow has been suggested by Lim et al. (2002). These authors have explored models of a jet produced with a slowly increasing ejection velocity, and find that the leading working surface can then set in motion a substantial amount of molecular environmental material (without dissociating it). However, it is not clear whether this material ends up being entrained into the main body of the jet, or whether it eventually also forms

an envelope around the jet beam.

Völker et al. (1999) have taken a simpler approach. These authors directly assume that the jets are injected with a partially molecular composition, and then calculate the excitation and dissociation of H_2 in the internal working surfaces which result from a time-variability of the ejection velocity. These models do produce spatially coincident atomic/ionic and molecular knots, corresponding to the successive internal working surfaces, qualitatively resembling the structures observed along the HH 111 and HH 1 jets. This success of the models of Völker et al. (1999) at reproducing the properties of HH 111 and HH 1 make them very attractive, so that we feel that they deserve further study.

If we want to justify this kind of model, we have to answer the question of whether or not an initially atomic wind (or jet) can generate an at least partially molecular constitution downstream. This question has been addressed by Rawlings, Williams, & Cantó (1988), who modeled the formation of molecules in a dust-free wind from a T Tauri star, and concluded that for mass loss rates $\dot{M} \sim 10^{-8} \rightarrow 10^{-7} M_\odot \text{ yr}^{-1}$ the fraction of H present as H_2 molecules is very low. Glassgold et al. (1989) computed similar models, but with higher mass loss rates, and concluded that a spherical wind with $\dot{M} \sim 10^{-5} \rightarrow 10^{-4} M_\odot \text{ yr}^{-1}$ does produce substantial molecular abundances. However, such mass loss rates are too high by 2–3 orders of magnitude compared to the rates appropriate for HH flows.

The models of spherical, dust-free winds from T Tauri stars used by Rawlings et al. (1988) and by Glassgold, Mamon, & Huggins (1989) in order to model molecule formation have now been replaced by the more sophisticated MHD “disk wind” models (in which the wind comes from the surface of an accretion disk, or from close to the accretion disk/stellar magnetosphere interface). A number of authors (Safier 1993; Shang et al. 2002; García et al. 2001) have studied the ionization state of the gas in these winds, but they have not discussed the possibility of forming molecules within the outflows. However (S. Lizano, private communication), it appears that the conclusions of Rawlings et al. (1988) and Glassgold et al. (1989) still hold for these more evolved “MHD disk wind” models, namely that mass loss rates $\dot{M} \geq 10^{-5} M_\odot \text{ yr}^{-1}$ are required for molecules to form in the wind. This issue will become more clear when papers on this subject begin to appear in the literature.

In the present paper we explore another possibility: that the sites of molecule formation in a dust-

free HH flow are the internal working surfaces. Raga et al. (1990) suggested such working surfaces (which result from a time-variability of the ejection velocity) as a possible model for the aligned knots along HH jets, and more recently, high angular resolution observations (see, e.g., Reipurth et al. 1997) appear to have confirmed this model at least for some HH flows.

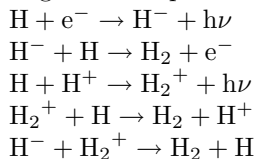
Internal working surfaces in radiative jets have high densities (resulting from the compression in the radiative shocks) and warm temperatures (typically of a few thousand K), which appear to be appropriate for the formation of H₂ in a dust-free, partially ionized gas through the reaction chains explored by Rawlings et al. (1988). In the present paper, we discuss calculations which include the dynamics and chemistry of a jet from a variable source, and we explore a limited parameter range (centered on a set of parameters that appears to be appropriate for the HH 1 jet) in order to find whether or not a substantial fraction of H₂ is produced. We then carry out predictions of the H α and the H₂ 1–0 S(1) emission in order to be able to compare our models with the observations of Reipurth et al. (2000).

In §2, we describe the chemical network that we have considered for our models. In §3, we describe the numerical setup for the integration of the gas-dynamic+chemical rate equations. In §4, a set of parameters is chosen, so as to model the emission along an HH jet. The results from these models are then presented in §§5, 6.

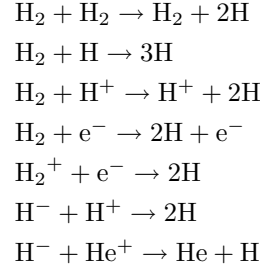
2. THE CHEMICAL NETWORK

We will assume that outflows from young stars are dust-free, and that they are not subjected to a substantial radiative field. Rawlings et al. (1988) have shown that in such a situation the formation of H₂ is dominated by negative ion and positive ion chemistries. In our simulations, we have considered the following set of species : H, H⁺, He, He⁺, He⁺⁺, C⁺, C⁺⁺, C³⁺, O, O⁺, O⁺⁺, H₂, H⁻, and H₂⁺.

We have included the collisional ionization, radiative+dielectronic recombination and charge exchange processes of the atoms and positive ions of H, He, C, and O in the way described by Raga et al. (2002a). We have also included the formation of H₂ via negative and positive ion chemistry:



as well as the destruction and charge exchange processes:



We have used the values for the rates from the RATE2000 UMIST data base (Le Teuff, Millar, & Markwick 2000). We have chosen logarithmic elemental abundances of (12, 11.0, 8.5, 8.8) for (H, He, C, O), respectively.

We have not included any photoreactions. In this, our chemical network differs from the one of Rawlings et al. (1988), who modeled the chemistry at the base of a T Tauri wind, where the stellar radiation field plays an important role. However, in the context of the present paper we are interested in the chemistry taking place at thousands of AU from the star, where the stellar radiation field is strongly diluted. The lack of photoreactions strongly affects the abundances of the H⁻ and H₂⁺ species, and allows them to initiate a strong H₂ formation sequence, unlike the situation found in the models of Rawlings et al. (1988). It is possible to show with simple analytic estimates that the reaction network described above will indeed lead to the formation of a substantial amount of H₂ in the conditions found in internal working surfaces of HH jets.

We should note that in our network it is assumed that C is at least singly ionized. This provides a seed electron density which feeds the beginning of the collisional ionization cascade of H. This assumption of singly ionized C at first sight appears to be inconsistent with the “zero radiative field” assumption of our chemical network. A possible way to justify the ionization of C is to assume that it was made close to the surface of the star, where the jet material *originates. At this location, the radiation field emitted by the star and/or by accretion shocks could easily lead to a full ionization of C into C⁺.

It is possible to show that if carbon is fully ionized to C⁺ close to the star, the ionization fraction will be “frozen in” in the expansion away from the stellar surface out to the $\sim 10^{15}$ cm diameter of an HH jet. If one considers a spherical, isothermal, constant velocity wind with initially fully ionized carbon, with a mass loss rate \dot{M} and a velocity v_w , which expands from an initial radius R_0 out to infinity (i.e., to the much larger radius of an HH jet), one can show that the final ionization fraction f_C in the wind is given

by

$$f_C = \left[1 + \frac{y_C \alpha_C \dot{M}}{1.3 m_H 4\pi R_0 v_w^2} \right]^{-1} = \left[1 + 0.13 \left(\frac{\dot{M}}{10^{-7} M_\odot \text{ yr}^{-1}} \right) \left(\frac{10 R_\odot}{R_0} \right) \left(\frac{200 \text{ km s}^{-1}}{v_w} \right)^2 \right]^{-1}, \quad (1)$$

where y_C is the abundance (by number) of carbon, m_H is the mass of hydrogen, and α_C is the coefficient of recombination to neutral carbon. The second equality has been obtained considering the C abundance that we have used for our simulations, an $\alpha_C = 4.7 \times 10^{-13} \text{ cm}^3 \text{ s}^{-1}$, and an initial radius for the wind of $10 R_\odot$. From this equation, it is clear that for the parameters of our HH jet models (see Table 1), the jet will indeed have a C^+ ionization fraction of $f_C \sim 1$, of course provided that C is singly ionised at the base of the wind.

With the temperatures and the densities of the different species resulting from the numerical models which we have carried out (see §3), we can then compute the emission coefficients of different emission lines. In particular, we focus on the $\text{H}\alpha$ and H_2 1–0 S(1) (2.12 μm) lines.

For the $\text{H}\alpha$ line, we compute an emission coefficient by considering the effective recombination coefficient for this line, and the population of the $n = 3$ level resulting from $n = 1 \rightarrow 3$ collisional excitations. We calculate the H_2 1–0 S(1) emission using a detailed model of the H_2 molecule (A. J. Lim, S. Tiné, J. M. C. Rawlings, and D. A. Williams, in preparation) which considers levels of the H_2 molecule below 36,000 K (211 levels in total). Although this model is capable of a non-equilibrium treatment of the level populations, this is prohibitively expensive for these simulations, and we have therefore “post-processed” the models to obtain the H_2 emission maps. We iterate the H_2 level populations to equilibrium (using a Runge-Kutta algorithm) for each cell in the numerical model. It is then easy to extract the 1–0 emission coefficient which is used to make the images in Figs. 5 and 6.

3. THE NUMERICAL SIMULATIONS

We have carried out numerical integrations of the 2D, axisymmetric gasdynamic equations together with the chemical network described in §2 with the “yguazú-a” binary adaptive grid code. This code has been described in detail by Raga et al. (2000) and extensively tested with laboratory experiments of laser-generated explosions (Sobral et al. 2000; Velázquez et al. 2001) and jets (Raga et al. 2001).

In particular, we have used the version of the code described by Raga et al. (2002a), which includes the radiative cooling due to the different processes associated with H_2 , H, H^+ , C^+ , C^{++} , O, O^+ , and a parametrized cooling for high temperatures, as well as the cooling due to collisional ionization of H and dissociation of H_2 . To this cooling scheme, we have now added the cooling processes associated with atomic and ionic He.

The numerical simulations are carried out in a 5-level, binary adaptive grid with a maximum resolution of $(3.91, 3.91) \times 10^{13} \text{ cm}$ (for models M1-M4, see Table 1 and §4) along the axial and radial (z, r) axes. In the $z = 0$ boundary, a “top hat” jet of outer radius r_j is injected with a time-independent density ρ_j and temperature T_j , and a variable velocity of the form:

$$v_0(t) = v_j + \Delta v_j \sin\left(\frac{2\pi t}{\tau}\right), \quad (2)$$

where t is the time and v_j , Δv_j , and τ are constants. We consider such a sinusoidal form for the time-dependent ejection velocity because we do not have a clear idea of what would be the correct functional form for modeling the knots along HH jets (this point has only been explored for the two well studied objects HH 111 and HH 34, see Masciadri et al. 2002 and Raga et al. 2002b).

On the $z = 0$, $r > r_j$ boundary we impose a reflection condition, as well as on the $r = 0$ boundary. We impose a free outflow condition on the other two boundaries of the computational domain.

4. PARAMETERS FOR THE HH 1 JET

In order to compute models of H_2 formation in the internal working surfaces of an HH jet, we first consider what parameters are appropriate for such flows. To this effect, we discuss the parameters that have been deduced from observations of HH 34, HH 111, and in particular the HH 1 jet, for which the most detailed comparison of the H_2 and atomic emission morphologies has been carried out (Reipurth et al. 2000).

Even though the HH 1 jet is seen in older images of the HH 1/2 system, it appears that its importance was first brought to attention by Strom et al. (1985). The HH 1 jet is composed of a chain of aligned knots which extends out to $\sim 25''$ away from the VLA 1 radio continuum source (which is thought to be the source of the HH 1/2 outflow, see Pravdo et al. 1985 and Rodríguez et al. 2000).

The proper motions of this chain of knots has been measured by Eislöffel, Mundt, & Böhm (1994) and more recently by Bally et al. (2002, from *HST*

images), who found that all of the knots have almost identical proper motions of $v_p \approx 325 \text{ km s}^{-1}$. These proper motions correspond to the spatial velocity of the knot, since the HH 1/2 axis lies almost on the plane of the sky (see, e.g., Böhm & Solf 1985).

The separations between the successive knots have values of $\Delta x \approx 0''.55$ (see, e.g., Reipurth et al. 2000). If one interprets these knots in terms of a variable ejection velocity jet model, one would then deduce an ejection variability period $\tau = \Delta x/v_p \approx 3.7 \text{ yr}$ (assuming a distance of 460 pc to HH 1).

We note that the knots close to the source along HH 34 have lower proper motions, with values of $\approx 200 \text{ km s}^{-1}$ (see Reipurth et al. 2002), and that the separations between successive knots imply a period of $\approx 30 \text{ yr}$. The knots along HH 111 have velocities of $\approx 300 \text{ km s}^{-1}$ (Hartigan et al. 2001), and can be modeled with a $\approx 60 \text{ yr}$ ejection velocity variability period (Raga et al. 2002c).

The H₂ 1–0 S(1) images obtained with the NICMOS camera of the *HST* by Reipurth et al. (2000) show that at $\approx 5''$ from the outflow source the HH 1 jet has a diameter of $\approx 150 \text{ AU}$ (corresponding to a radius of $\approx 1.1 \times 10^{15} \text{ cm}$), and that the jet widens to $\approx 300 \text{ AU}$ at $10''$ from the source. Radii of $\sim 2.5 \times 10^{15} \text{ cm}$ are observed for the HH 34 (Reipurth et al. 2002) and HH 111 jets (Hartigan et al. 2001).

Strom et al. (1985) have used the [S II] 6716/6730 line ratio to determine an electron density $n_e \approx 4 \times 10^3 \text{ cm}^{-3}$ for the HH 1 jet. As is typical for an object with a low excitation spectrum, the ionization fraction along the HH 1 jet is very low (as initially pointed out by Brugel, Olmsted, & Böhm 1983), and one would have to multiply n_e by a factor of $\sim 10^2 - 10^3$ in order to obtain the atom+ion number density in the working surfaces of the HH 1 jet. For the HH 34 jet, Raga & Noriega-Crespo (1998) have carried out numerical simulations of the outflow, and they find that in order to reproduce the observed H α and red [S II] line fluxes one needs to have an initial density of atoms+ions of $\sim 5 \times 10^4 \text{ cm}^{-3}$.

For our numerical simulations, we have chosen an $r_j = 5 \times 10^{14} \text{ cm}$ initial jet radius. This radius approximately corresponds to an extrapolation to the position of the source of the position-dependent width of the HH 1 jet (see above and Reipurth et al. 2000). As discussed in §2, we assume that we have a sinusoidal ejection velocity variability (see Eq. 2) for which we choose a mean velocity $v_0 = 200 \text{ km s}^{-1}$ and a period $\tau = 10 \text{ yr}$. These parameters are intermediate between the ones deduced for the HH 1 jet knots (which have a velocity of $\sim 300 \text{ km s}^{-1}$ and

a period of $\sim 4 \text{ yr}$) and the ones of the HH 34 and HH 111 jets.

We also have to choose the half-amplitude Δv_j for the assumed sinusoidal ejection velocity variability. While there are no estimates of this parameter for the HH 1 jet, Raga & Noriega-Crespo (1998) have estimated a $\Delta v_j = 15 \text{ km s}^{-1}$ for the chain of knots close to the HH 34 source. Raga et al. (2002b) used a lower $\Delta v_j = 10 \text{ km s}^{-1}$ value for the knots along HH 34, and a $\Delta v_j = 30 \text{ km s}^{-1}$ value for the knots of HH 111 (which apparently are formed by a “saw-tooth” time-dependent velocity variability, see Masciadri et al. 2002). We then choose three values for the velocity variability half-amplitude : $\Delta v_j = 10, 15$ and 20 km s^{-1} (see Table 1), which are representative of the range of values that might be relevant for producing the chains of knots along HH jets.

For the initial jet density, we have chosen two values, $n_j = 2 \times 10^5$ and $2 \times 10^6 \text{ cm}^{-3}$ (see Table 1). These values correspond to the electron density measured for the HH 1 jet multiplied by factors of 50 and 500 (respectively). Also, if we scale the density estimated for HH 34 by Raga & Noriega-Crespo (1998) to the radii and velocities of the HH 1 jet (so as to maintain the same value for the mass loss rate), we obtain a density of $\approx 10^6 \text{ cm}^{-3}$. Therefore, the density values that we have chosen appear to be representative of the values that could be present in the base of an HH jet (i.e., at a distance of a few hundred AU from the source). For all of the models, we assume that the jet is initially neutral, except for C which is assumed to be singly ionized.

Finally, we impose an initially neutral (except for C which is assumed to be singly ionized), homogeneous environment of density $n_{env} = 10^3 \text{ cm}^{-3}$ and temperature $T = 10^3 \text{ K}$. This is of course an oversimplification of the situation actually found in objects like HH 1 or HH 111, which are clearly seen to be emerging from a dense cloud core into a more diffuse environment.

With the parameters discussed above, we have chosen to run four models which share most of the model parameters (namely, the same environment, initial jet temperature, radius, mean velocity and variability period), except for the amplitude of the velocity time-variability and the initial density of the jet. The combinations of parameters chosen for the four models (models M1,...,M4) are given in Table 1.

5. MODEL PREDICTIONS

We have integrated the gasdynamical+chemical rate equations for the four variable ejection velocity jet models listed in Table 1 and §4. The four models

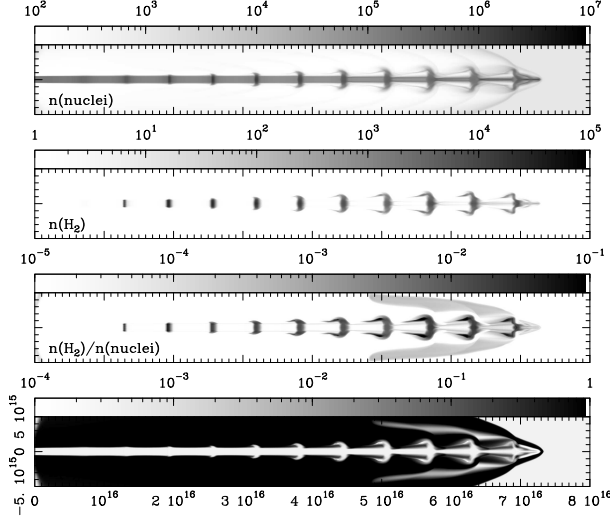


Fig. 1. Density (of atomic nuclei), H_2 density, H_2 fractional abundance (relative to the total number of nuclei), and electron density fractional abundance obtained for model M1 (see §4 and Table 1) after a $t = 120$ yr time integration. The stratifications are depicted with the logarithmic greyscales shown by the bars above each plot (the densities being labeled in cm^{-3}). The axial (abscissa) and radial (ordinate) coordinates are labeled in cm. The length along the symmetry axis is 8×10^{16} cm.

were integrated forward in time for 120 yr, by which time the leading working surfaces of the jets have travelled through most of the computational domain.

Figure 1 shows the stratifications of the density (of atomic nuclei), H_2 number density, molecular fraction and ionization fraction resulting from the time-integration of model M1. The maximum density (of atomic nuclei, with a value of $1.5 \times 10^6 \text{ cm}^{-3}$) is found in the working surface located at $z \approx 2.6 \times 10^{16}$ cm, and the maximum H_2 density (with a $2.7 \times 10^4 \text{ cm}^{-3}$ value) is found in the working surface located at $z \approx 1.9 \times 10^{16}$ cm. The maximum fraction of H nuclei in the form of H_2 has a value of 0.05 (in the working surface at $z \approx 1.9 \times 10^{16}$ cm), and the fractional abundance of H_2 has a similar order of magnitude for all of the other internal working surfaces (see Figure 1). The ionization fraction (lower plot of Fig. 1) has low on-axis values of $\sim 10^{-4}$ for all of the internal working surfaces, but reaches values of ~ 1 (i.e., fully ionized hydrogen) in the wings of all of the working surfaces with $z > 4 \times 10^{16}$ cm.

Model M2 produces stratifications with morphologies similar to the ones of model M1, but with densities (of nuclei) and electron densities larger by a factor of ~ 10 (see Figure 2). The H_2 molecular fraction has values of ~ 0.1 for all of the internal working surfaces. Model M3 (see Figure 3) also has similar

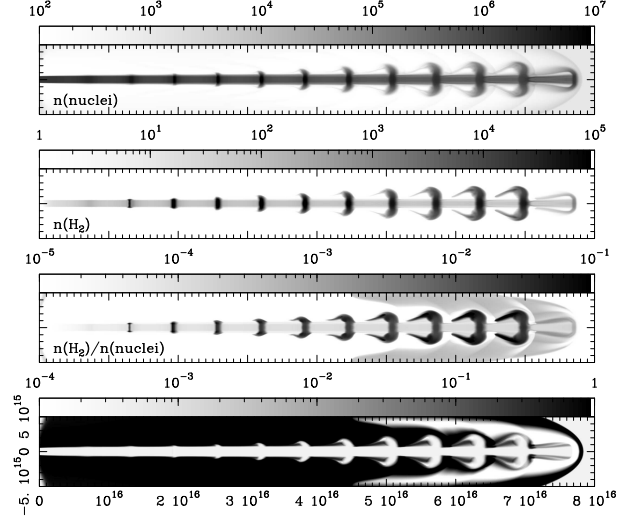


Fig. 2. Same as Fig. 1, but for model M2 (see §4 and Table 1).

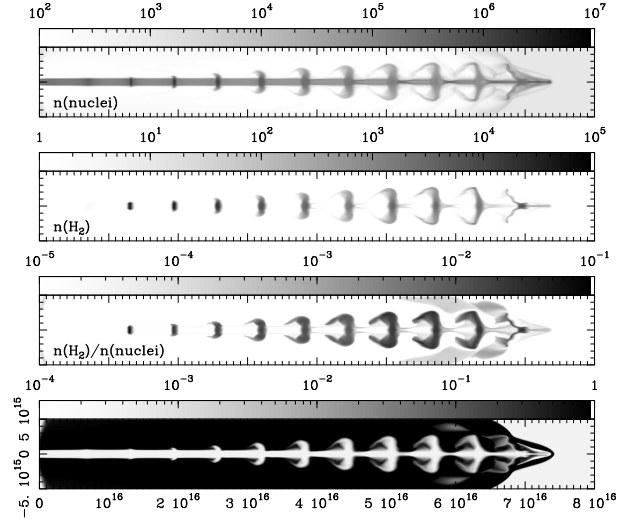


Fig. 3. Same as Fig. 1, but for model M3 (see §4 and Table 1).

H_2 fractions in all of the internal working surfaces, but with lower values of ~ 0.02 .

Model M4 (see Figure 4) produces an H_2 fraction of ~ 0.05 only in the first working surface (at $z \approx 7 \times 10^{15}$ cm) and low values ($< 10^{-3}$) for all of the working surfaces farther away from the source. This is a direct result of the fact that the working surface shocks heat the gas to temperatures that are too high for H_2 molecules to survive.

In model M4, as the working surfaces start to develop and grow in shock velocity, H_2 starts to form. However, when the shock velocities reach values of above $\sim 10 \text{ km s}^{-1}$ (as the working surfaces travel down the jet flow), the temperature is high enough

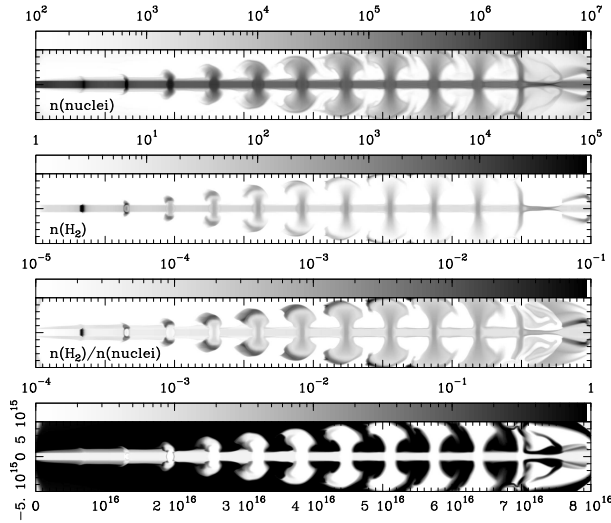


Fig. 4. Same as Fig. 1, but for model M4 (see §4 and Table 1).

for the dissociation processes to become active, and the net production of H₂ drops in a substantial way. The H₂ that was produced earlier in the evolution of the working surfaces ends up being ejected sideways from the jet beam, and forms a ring-like structure surrounding the working surfaces (see the knots with $z > 2 \times 10^{16}$ cm in Fig. 4).

6. H α AND H₂ 1-0 S(1) EMISSION MAPS

From the four models described in §5 (also see Table 1), we have computed the H α and H₂ 1-0 S(1) (2.12 μ m) emission coefficients (see §2), and integrated them through lines of sight in order to obtain predictions of intensity maps for these two emission lines. In order to compute the maps, we assume that the outflow axis lies on the plane of the sky.

In Figure 5, we show cuts of the H α and H₂ 1-0 S(1) emission maps along the outflow axis for the four models that we have computed. In model M1, the H₂ emission dominates over the H α emission by 1-3 orders of magnitude for all of the knots with $z < 4 \times 10^{16}$ cm. We then find four knots (with $4 \times 10^{16} < z < 6.5 \times 10^{16}$ cm) that have comparable (i.e., within an order of magnitude) H α and H₂ emission. Finally, the leading working surface (which is being caught up by one of the internal working surfaces) has a dominant H α emission.

In model M2 (see Fig. 5), the H₂ emission completely dominates over the H α emission for all of the knots with $z < 5.5 \times 10^{16}$ cm, and has comparable H α and H₂ emission in the three leading internal working surfaces. Model M3 shows an emission structure which resembles model M2 (see Fig. 5).

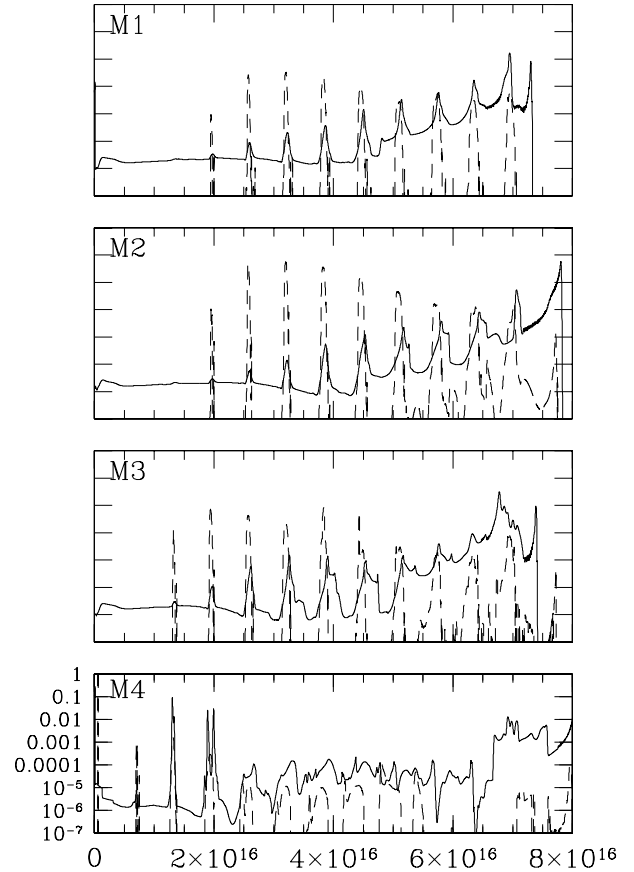


Fig. 5. Cuts along the outflow axis of the H α (solid lines) and H₂ 1-0 S(1) (dashed lines) intensity maps obtained from the four computed jet models (see §§4, 5, 6, and Table 1). The intensity maps were computed assuming that the outflow axis lies on the plane of the sky, from the flow stratifications obtained for a $t = 120$ yr time-integration. The intensities are given in $\text{erg cm}^{-2} \text{s}^{-1} \text{sterad}^{-1}$ units, and the position z along the outflow (horizontal) axis is in cm.

Finally, in model M4 the two working surfaces closer to the source (i.e., with $z < 1.5 \times 10^{16}$ cm) have comparable H₂ and H α emission (and very weak H α). The internal working surfaces at larger distances from the source ($z > 2.5 \times 10^{16}$ cm) show only faint, on-axis emission, but with H α dominating over H₂ by ~ 1 order of magnitude.

From the point of view of modeling jets such as HH 1 and HH 111, which show a chain of knots which are visible in both H α and in the H₂ 1-0 S(1) lines (see Reipurth et al. 2000 and Gredel & Reipurth 1994), model M1 appears to be the more appropriate one. Therefore, we conclude that a model with a sinusoidal velocity variability with a half-amplitude $\Delta v_j \approx 10 \text{ km s}^{-1}$ and a mass loss rate

$\dot{M} \approx 10^{-7} M_{\odot} \text{yr}^{-1}$ (see Table 1) appears to be appropriate for modeling these HH flows.

Model M2 (with identical parameters to model M1, but with a higher density resulting in a $\dot{M} \approx 10^{-6} M_{\odot} \text{yr}^{-1}$ mass loss rate, see Table 1) or Model M3 (with a higher velocity variability amplitude) could be appropriate for modeling some of the so-called H₂ jets (e.g., the well studied HH 212, see Davis et al. 2000b and references therein), which show only very weak (or are not detected in) atomic/ionic lines.

Model M4, is an example of a parameter combination which does not produce an observable chain of aligned H₂ knots. From the results obtained from this model, we deduce that in order to produce several H₂ knots one needs a model with a time-dependent ejection velocity of rather low amplitude (see Table 1).

In Figure 6, we show the H α and H₂ 1–0 S(1) intensity maps obtained from model M1. From this figure it is clear that the model produces several knots which could be detected both in the H α and in the H₂ emission (as is also seen in the axial cuts of the emission which are shown in Fig. 5). One can also see that the radial extent (i.e., the width) of the knots is similar in both the H α and the H₂ emission, which is in qualitative agreement with the observations of the HH 1 jet of Reipurth et al. (2002).

We should point out that some of the features seen in the H α emission are not computed correctly in our numerical models. In the regions immediately after shock waves moving into a neutral medium, collisionally excited H α emission is produced. These regions can be seen as sharp “spikes” in the H α emission vs. position cuts shown in Fig. 5. The regions with collisionally excited H α , however, typically have

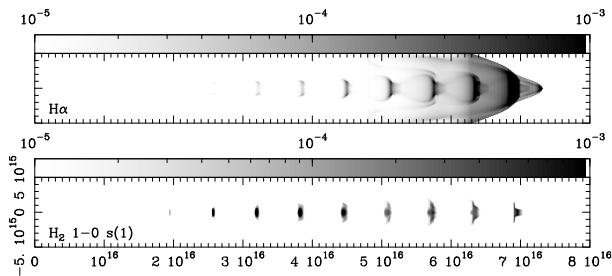


Fig. 6. H α (top) and H₂ 1–0 S(1) (bottom) intensity maps computed from model M1 (see Table 1 and §5) after a $t = 120$ yr time-integration. It has been assumed that the outflow axis lies on the plane of the sky. The intensities are depicted with the logarithmic greyscale given on the top of the graph (labeled in units of $\text{erg cm}^{-1} \text{s}^{-1} \text{sterad}^{-1}$). The axes are labeled in cm.

spatial extents smaller than our computational resolution by a factor of ~ 10 . Therefore the computed intensities of these H α spikes are completely unreliable.

7. CONCLUSIONS

In this paper, we have re-analyzed the formation of molecules (in particular, of H₂) in outflows from young stars in the context of models of jets from variable sources. This work is to some extent a continuation of the work of Rawlings et al. (1988) and Glassgold et al. (1989), who had studied molecule formation in isotropic, steady winds from T Tauri stars.

We have explored a limited set of parameters for models of a jet with a sinusoidally time-varying ejection velocity. This is of course a quite limiting assumption, particularly since there appears to be observational evidence that a range of functional forms are possible for the ejection time-variabilities that give rise to internal working surfaces in HH jets (see Raga et al. 2002b). The parameters that we have explored (see Table 1) are representative of the properties deduced for the chains of aligned knots along the HH 1, HH 34, and HH 111 jets (see §3).

From our models, we find that (for appropriate flow parameters) internal working surfaces can be the sites of formation of a substantial amount of H₂ (with fractional abundances of up to $\sim 10\%$). Also, these working surfaces can produce strong H₂ emission, which can be comparable to or even greater than the H α emission (see §6).

In particular, we find that a model with an ejection velocity variability half-amplitude $\Delta v_j = 10 \text{ km s}^{-1}$ and an average mass loss rate $\dot{M} \approx 10^{-7} M_{\odot} \text{yr}^{-1}$ (model M1 of Table 1) produces a chain of knots which have comparable (within an order of magnitude) H α and H₂ 1–0 S(1) emission (see §6). Such a model appears to be appropriate for objects such as HH 1 and HH 111, which have a chain of knots which are detected in these two emission lines (Reipurth et al. 2000; Gredel & Reipurth 1994).

For larger values of \dot{M} (model M2, see Table 1 and §5), we obtain knots which have high H₂ 1–0 S(1)/H α line ratios. However, if we raise the value of Δv_j above 20 km s^{-1} (model M4, see Table 1), the H₂ emission basically vanishes in all of the knots except in the ones closest to the outflow source (see §6). From this result, we conclude that the H₂ emission is very sensitive to the amplitude of the outflow velocity variability Δv_j (see Eq. 1). Therefore, only the HH jets ejected with low enough values of Δv_j should show chains of aligned, H₂ emitting knots.

TABLE 1

PARAMETERS OF THE VARIABLE JET MODELS DESCRIBED IN THE TEXT

Model	Δv_j^a [km s ⁻¹]	n_j^b [cm ⁻³]	\dot{M}_j^c [M_\odot yr ⁻¹]
M1	10	2×10^5	1.1×10^{-7}
M2	10	2×10^6	1.1×10^{-6}
M3	15	2×10^5	1.1×10^{-7}
M4	25	2×10^5	1.1×10^{-7}

^aHalf-amplitude of the sinusoidal velocity variability. All of the models have a $v_0 = 200$ km s⁻¹ average velocity, and a $\tau = 10$ yr variability period.

^bTime-independent injection number density. All of the models have a $T_j = 10^3$ K injection temperature and a $r_j = 5 \times 10^{14}$ cm initial radius.

^cTime-averaged mass loss rate.

We feel that our general result that a substantial fraction of H₂ can be formed in internal working surfaces of HH jets is indeed correct. However, the conclusions that we have obtained with respect to the parameters necessary for substantial H₂ formation to occur are not so certain.

An important matter of concern is the nature of the time-variability of the ejection. We have only explored jets ejected with a constant density and a sinusoidal velocity variability. Other kinds of time-dependent ejection might lead to different requirements for the parameters necessary for H₂ formation.

Another important fact is that our models are purely gasdynamical, and do not include the effects of magnetic fields. As has been well studied in the literature, the presence of a magnetic field (with a nonzero component parallel to the shock waves present in the flow) leads to lower post-shock temperatures, and can have a strong effect on the destruction (and formation) of H₂. This is particularly true for shock waves in the 10–30 km s⁻¹ velocity range, such as are present in our jet models (see, e.g., the work of Smith, Brand, & Moorhouse 1991). These effects clearly deserve further study.

The presence of a magnetic field would increase the values of the ejection velocity variability amplitudes which lead to the formation of H₂ emitting knots (with respect to what we find with our purely gasdynamical models). However, it is unlikely that our model could explain (even with the aid of a moderately strong magnetic field) objects like the particularly dramatic HH 46/47, which has a bright

internal working surface (HH 47A) with strong H₂ emission and associated shock velocities of close to 100 km s⁻¹ (see, e.g., Curiel et al. 1995). For such high shock velocity working surfaces, the observed molecular gas probably has to correspond to entrained material.

AR acknowledges support from the CONA-CyT grants 36572-E, 41320-F and 43103-F and the DGAPA (UNAM) grants IN 112602 and IN 111803. AJL acknowledges support from PPARC for a post-doctoral research assistantship, and DAW is grateful to the Leverhulme Trust for a travel grant. AR acknowledges I. Díaz for his support with the computing facilities with which the numerical simulations were carried out. We thank an anonymous referee for relevant comments.

REFERENCES

- Bally, J., Heathcote, S., Reipurth, B., Morse, J., Hartigan, P., & Schwartz, R. 2002, *AJ*, 123, 2657
- Böhm, K. H., & Solf, J. 1985, *ApJ*, 294, 533
- Brugel, E. W., Olmsted, E., & Böhm, K. H. 1983, *A&A*, 125, 23
- Curiel, S., Raymond, J. C., Wolfire, M., Hartigan, P., Morse, J., Schwartz, R. D., & Nisenson, P. 1995, *ApJ*, 453, 222
- Davis, C. J., Berndsen, A., Smith, M. D., Chrysostomou, A., & Hobson, J. 2000b, *MNRAS*, 314, 241
- Davis, C. J., Eislöffel, J., & Smith, M. D. 1996, *ApJ*, 463, 246
- Davis, C. J., Mundt, R., & Eislöffel, J. 1994, *ApJ*, 437, L55
- Davis, C. J., Smith, M. D., & Eislöffel, J. 2000a, *MNRAS*, 318, 747
- Downes, T. P., & Cabrit, S. 2003, *A&A*, 403, 135
- Eislöffel, J., Mundt, R., & Böhm, K. H. 1994, *AJ*, 106, 1042
- Fernandes, A. J. L. 2000, *MNRAS*, 315, 657
- García, P. J. V., Ferreira, J., Cabrit, S., & Binette, L. 2001, *A&A*, 377, 589
- Glassgold, A. E., Mamon, G. A., & Huggins, P. J. 1989, *ApJ*, 336, L29
- Gredel, R., & Reipurth, B. 1994, *A&A*, 289, L19
- Hartigan, P., Morse, J. A., Reipurth, B., Heathcote, S., & Bally, J. 2001, *ApJ*, 559, L157
- Le Teuff, Y. H., Millar, T. J., & Markwick, A. J., 2000, *A&AS*, 148, 157
- Lim, A. J., Raga, A. C., Rawlings, J. M. C., & Williams, D. A. 2002, *MNRAS*, 335, 817
- Masciadri, E., Velázquez, P. F., Raga, A. C., Cantó, J., & Noriega-Crespo, A. 2002, *ApJ*, 573, 260
- Noriega-Crespo, A., Garnavich, P. M., Raga, A. C., Cantó, J., & Böhm, K. H. 1996, *ApJ*, 462, 804
- Pravdo, S. H., Rodríguez, L. F., Curiel, S., Cantó, J., Torrelles, J. M., Becker, R. H., & Sellgren, K. 1985, *ApJ*, 293, L35

- Raga, A. C., Cantó, J., Binette, L., & Calvet, N. 1990, *ApJ*, 364, 601
- Raga, A. C., de Gouveia dal Pino, E. M., Noriega-Crespo, A., Mininni, P., & Velázquez, P. F. 2002a, *A&A*, 392, 267
- Raga, A. C., Navarro-González, R., & Villagrán-Muniz, M. 2000, *RevMexAA*, 36, 67
- Raga, A. C., & Noriega-Crespo, A. 1998, *AJ*, 116, 2943
- Raga, A. C., Noriega-Crespo, A., Reipurth, B., Garnavich, P. M., Heathcote, S., Böhm, K. H., Curiel, S., 2002c, *ApJ*, 565, L29
- Raga, A. C., Sobral, H., Villagrán-Muniz, M., Navarro-González, R., & Masciadri, E. 2001, *MNRAS*, 324, 206
- Raga, A. C., Velázquez, P. F., Cantó, J., & Masciadri, E. 2002b, *A&A*, 395, 647
- Rawlings, J. M. C., Williams, D. A., Cantó, J., 1988, *MNRAS*, 230, 695
- Reipurth, B., Hartigan, P., Heathcote, S., Morse, J. A., & Bally, J. 1997, *AJ*, 114, 757
- Reipurth, B., Heathcote, S., Morse, J., Hartigan, P., & Bally, J. 2002, *AJ*, 123, 362
- Reipurth, B., Heathcote, S., Yu, K. C., Bally, J., & Rodríguez, L. F. 2000, *ApJ*, 534, 317
- Reipurth, B., & Olberg, M. 1991, *A&A*, 246, 535
- Reipurth, B., Raga, A. C., & Heathcote, S. 1996, *A&A*, 311, 989
- Rodríguez, L. F., Delgado-Arellano, V. G., Gómez, Y., Reipurth, B., Torrelles, J. M., Noriega-Crespo, A., Raga, A. C., & Cantó, J. 2000, *AJ*, 119, 882
- Safer, P. N. 1993, *ApJ*, 408, 115
- Shang, H., Glassgold, A. E., Shu, F. H., & Lizano, S. 2002, *ApJ*, 564, 853
- Smith, M. D., Brand, P. W. J. L., & Moorhouse, A. 1991, *MNRAS*, 248, 451
- Sobral, H., Villagrán-Muniz, M., Navarro-González, R., & Raga, A. C. 2000, *App.Phys.Lett.*, 77, 3158
- Strom, S. E., Strom, K. M., Grasdalen, G. L., et al. 1985, *AJ*, 90, 2281
- Velázquez, P. F., Sobral, H., Raga, A. C., Villagrán-Muniz, M., & Navarro-González, R. 2001, *RevMexAA*, 37, 87
- Völker, R., Smith, M. D., Suttner, G., & Yorke, H. W. 1999, *A&A*, 343, 953

Andrew J. Lim: Department of Applied Mathematics, University of Leeds, LS2 9JT, United Kingdom
(ajl@ast.leeds.ac.uk).

Alejandro C. Raga: Instituto de Ciencias Nucleares, UNAM, Apdo. Postal 70-543, 04510 México, D. F., México
(raga@nuclecu.unam.mx).

David A. Williams: Department of Physics and Astronomy, UCL, Gower St., London, WC1E 6BT, United Kingdom
(daw@star.ucl.ac.uk).